

Numerical Investigation of Fluid Flow and Heat Transfer in a Two-Pass Channel with Perforated Ribs

Arjumand Rasool* and Adnan Qayoum

Department of Mechanical Engineering, National Institute of Technology Srinagar, Kashmir, 190006, India

ABSTRACT

Rib turbulators are largely utilized for enhancement of heat transfer in cooling channels of gas turbine blades. The present study focuses on the heat transfer, fluid flow and pressure drop study of perforated ribs fixed to the bottom wall of a two-pass square channel. The turbulent flow details for heat transfer and fluid flow for perforated ribs are simulated by using commercial software Comsol 5.3a with an established turbulence model i.e. Standard k- ϵ . The assiduity is towards analyzing the possible effects of varying inclination angle (0 to 30°) and shape of hole (cylinder to square) on heat transfer and friction factor characteristics for turbulent flow. The studied Reynolds number varies from 10000 to 50,000. Computations are carried out to determine inter-rib distribution of local heat transfer coefficient over the bottom ribbed wall. The phenomenon responsible for the heat transfer enhancement by perforated ribs is delineated. The results reveal that perforated ribs lead to enhancement of local heat transfer distribution (Nu/Nu_0) on the end wall downstream the ribs. Perforated ribs develop longitudinal vortices. These vortices cause an increase in flow mixing and turbulent kinetic energy. The square perforated ribs provide a 37.1–57.3% higher normalized average Nusselt number relative to the solid ribs, however induce high pressure drop. Overall, square perforated ribs (Case-3) provide the best thermal-hydraulic performance.

Keywords: Comsol, convective heat transfer, perforated ribs, turbine blade cooling, turbulence model

ARTICLE INFO

Article history:

Received: 1 March 2018

Accepted: 28 May 2018

Published: October 2018

E-mail addresses:

arjumand.beigh@yahoo.co.in (Arjumand Rasool)

adnan@nitsri.ac.in (Adnan Qayoum)

* Corresponding author

INTRODUCTION

Technological improvements in heat exchange processes are necessary for the thermal energy systems to combat the everyday increasing demand for power. Most of the thermal systems, particularly gas turbine blades operate under high inlet

temperatures (1200K-1700K) to ascertain the higher thermal efficiency. The present materials available for turbine blades are not able to withstand large periods of exposure to these harsh temperature conditions, even with thermal barrier coatings (TBC). Therefore, requires effective cooling methods. Since the introduction of turbine blade cooling, considerable improvements in increasing turbine inlet temperatures have been made. Internal passages of turbine blades are cooled by circulating air through them. These passages are connected by 180° bend. Various heat transfer enhancement (active/passive) techniques have been proposed to improve the internal cooling of thermal systems like gas turbine blade cooling, electronic systems, nuclear reactors and compact heat exchangers etc (Webb, 1994). The heat transfer enhancement and cooling techniques used in gas turbine are discussed in detail by (Han et al., 2012). For internal flows, large scale surface roughness including repeated ribs (Acharya et al., 1993; Han et al., 1985; Tariq et al., 2003) vortex generators (Liou et al., 2000; Yuan & Tao., 2003) and baffles/fins (Chamoli & Thakur, 2015; Gao et al., 2016) have been exhaustively employed for heat transfer augmentation. Rib turbulators on the channel walls are rigorously studied for heat transfer enhancement, however lead to a significant pressure drop. The presence of ribs produces typical flow patterns, which disrupts the laminar sub-layer and instigates boundary layer recreation, hence leads to heat transfer enhancement yet with additional pressure drop. In addition to pressure drop penalty, conventional (square/rectangular) rib turbulators possesses more affinity towards the hot-spots at the rear corners of the ribs, as well as at the juncture of ribs and side walls where corner eddies are formed and the flow becomes almost stagnant. These hot-spots can even lead to thermal failure in gas turbine blades. Thus, a large number of rib shapes with and without perforation have been tested which can overcome the problem of hot spot generation (Ali et al., 2016; Buchlin, 1993; Sharma et al., 2017; Tariq et al., 2004). Figure 1 shows the hot spot formation at the rear concave corner of square rib turbulators. Armellini et al. (2008) and Coletti et al. (2008) conducted both experimental and numerical study of a trapezoidal cross-section cooling duct having ribs on one wall and crossing jets. It had been found that the combined action of ribs and jets increased turbulent mixing and hence led to heat transfer enhancement. Shin and Kwak (2008) analyzed the heat transfer performance of ribbed cooling passage of gas turbines blade model with five different kinds of ribs. The results showed that arrangement of holes in staggered manner gave highest enhancement of heat transfer, yet friction factor increased greatly. They suggested to optimize the hole shape for getting maximum thermal performance of the perforated blockage. Ahn et al. (2007) performed an experiment using naphthalene sublimation technique to study mass transfer in rectangular channel with ribs having round and elongated holes. The hole aspect ratios, for each hole to channel area ratio, was analyzed. It was found that, ribs with elongated holes performed better than round

holes in terms of mass transfer. Chung et al. (2013) carried out an experiment to determine the effects of improved hole arrays on the thermal hydraulic performance of cooling channels. They concluded that an inclined hole array represented improved thermal hydraulic performance over the conventional center hole configuration. Liou et al. (1998) investigated the effect of permeable ribs on the heat transfer performance in the rectangular duct; the results showed that permeable ribs lead to abridged hot spot regions which usually occurred behind the solid rib, hence leading to significant heat transfer enhancement. Hwang and Liou (1994) reported that the inclination angle of perforation modified the transport nature of flow through jets greatly. The higher inclination angle of hole makes transport properties of the flow more effective. Thianpong et al. (2012) carried out a heat transfer and thermal performance study of a heat exchanger tube fitted with perforated twisted-tapes. They found that perforated twisted tapes caused a considerable increase in heat transfer rate in comparison to traditional twisted tapes. Jeng et al. (2013) experimentally studied the heat transfer performance of a 180° round turned channel with a perforated divider. The authors found that by adjusting the size and angle of perforation, these perforations could achieve spatial thermal regulation and enhance the total heat transfer rate. Qayoum and Panigrahi (2018) carried out an experimental investigation of a two-pass channel with permeable ribs using liquid crystal thermography technique. The researchers observed a tremendous enhancement of heat transfer with a split slit rib configuration, without any appreciable increase in pressure drop.

As the flow through channels with rib turbulators is highly complex and the internal nature of heat transfer coefficient, friction factor and hot spot formation are primarily controlled by the production and manipulation of large scale vortical structures induced due to modification in rib geometry. Therefore, it is of prime importance to get the detailed spatial and temporal information to understand the heat transfer and fluid flow mechanisms. Recent development in computational fluid dynamics based softwares allows engineers to acquire high resolution temporal and spatial information of temperature and flow field. In this regard Comsol 5.3a can be seen as a promising computational tool to get the detailed information of heat transfer characteristics in the pertinent field.

Pertinent literature as summarized above has scrutinized that perforated blockages can possibly improve hot spots and thermal hydraulic performance of the internal cooling passages. However, the above perforated ribs heat transfer performances have been limited to single pass channel only and no investigations have yet been reported in two-pass channels. Also, in the present study square perforation is introduced to study the impact of hole shape on heat transfer and pressure drop characteristics. The primary purpose of this study is to identify the best possible rib perforation within the range of parameter under investigation (i.e. Re) for enhancement of heat transfer at reduced pressure penalty, with

an aim of obviating the possible local hotspots. Based on the heat transfer coefficient and pressure drop measurements, the thermal performance factor for all the rib geometries are assessed in the current computation while utilizing the constant pumping power criteria (Webb and Eckert., 1972).

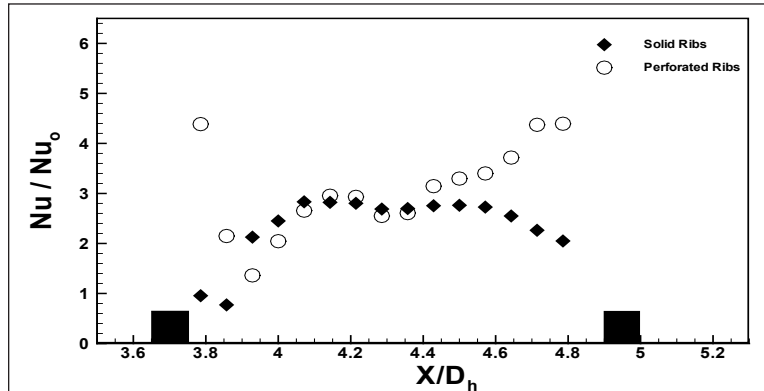


Figure 1. Normalized Nusselt number distribution behind solid and perforated rib turbulators

Numerical Simulation and Physical Model

Figure 2 shows the schematic diagram of computational domain used for present simulation. All the dimensions of the geometry are in mm. The present computational study includes all rib configurations (Case 1-5) as depicted in Table 1. However, only mesh of rib with cylindrical hole is presented in Figure 3. All the four tested perforated ribs differ only in geometry keeping the cross-sectional area same. The length (l) of the test section is 1000 mm and the cross-section is 140 mm x 140 mm. The bottom wall is heated with a constant temperature of 100°C for all the summary of cases studied. Ribs were periodically mounted on bottom heated wall, 5 in each pass. The pitch-to-rib height ratio (p/e) and the blockage ratio (e/D_H) of ribs are 8 and 0.15, respectively.

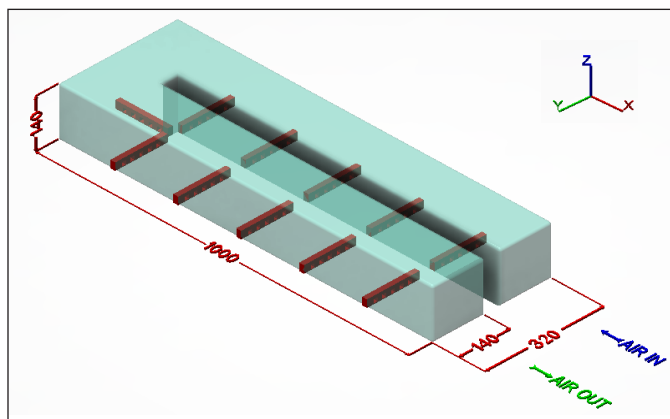
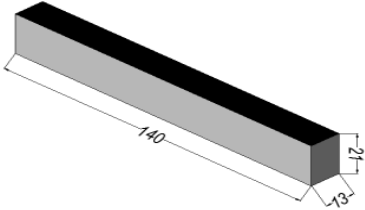
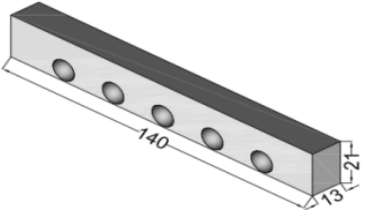
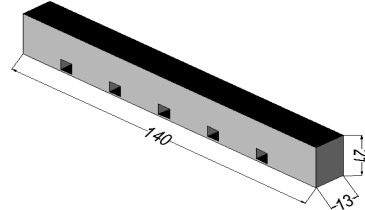
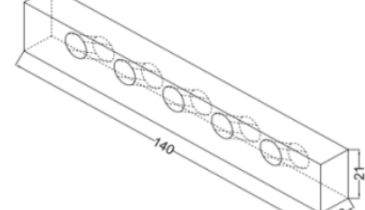
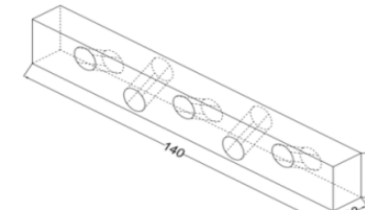
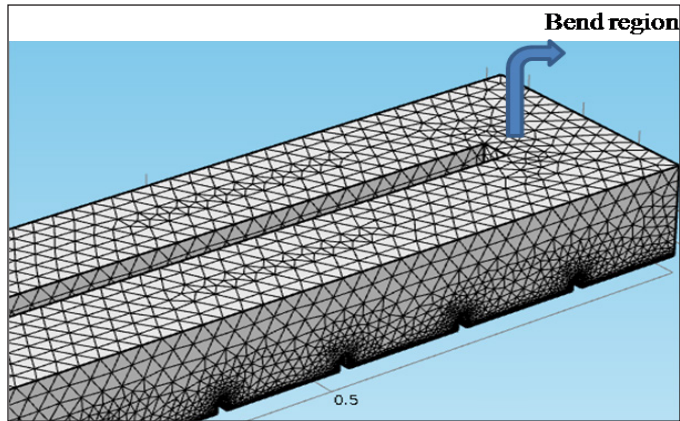


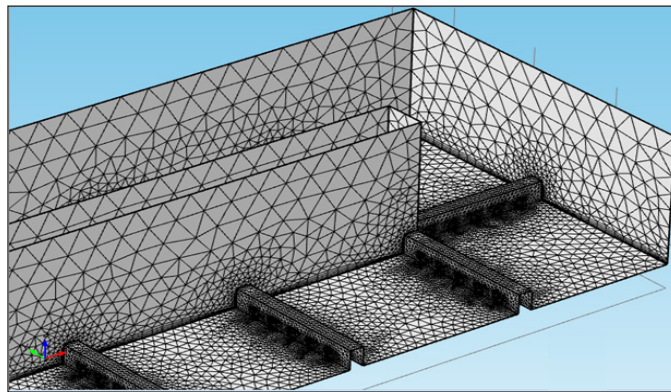
Figure 2. Geometry of a computational domain

Table 1
Construction details of different perforated rib configurations for current study

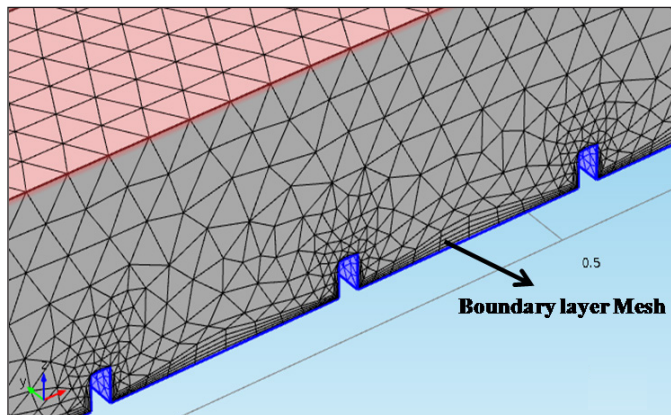
Test Cases	Rib Configuration	Rib Angle
Case 1		Solid Rib
Case 2		Cylindrical hole at bottom
Case 3		Square hole at bottom
Case 4		Cylindrical hole inclined at 30°
Case 5		Tilted cylindrical holes



(a)



(b)



(c)

Figure 3. (a) Overall view of the mesh and (b) Cut-section view of mesh for perforated ribs (c) Enlarged view of boundary layer mesh

Details of Computational Module and Procedure

The present numerical technique uses k- ϵ module of the commercial software Comsol 5.3a to simulate mean flow characteristics for turbulent flow conditions under specified boundary conditions. The k- ϵ module is a two-equation model, which by means of two Partial differential equations gives a broad portrayal of turbulence. The k- ϵ turbulence model provides accurate results of the physics and characteristics of most of the flows in industries, also it is found that it can predict the secondary flow and strong streamline curvature flows correctly. Therefore, the k- ϵ turbulence model is found to be favorable for the complex fluid flows in the ribbed ducts (Comsol user's guide 5.3a). Comsol 5.3a uses finite element method (FEM) to find approximate solutions of partial differential equations (PDE) and integral equations. A non-isothermal flow has been used where the fluid flow interface is coupled with the heat transfer interface, and pressure forces and the viscous dissipation rate of the fluid are considered. The summary of the steps the above numerical model used are as discretization of the continuous domain and coupled governing equations (elements type and size), generation and propagation of absolute and relative tolerances or errors for convergence criteria, formulating the nonlinear settings for iteration procedure and selection of the suitable solver approach.

In the current study a computational domain was meshed using simple linear free triangular mesh. Figure 3 depicts the overall and enlarged view of the mesh of computational domain. Same size of grid was used for all the cases studied, so as to ensure the homogeneity. The distance of nearest nodes from the wall was maintained to $(y^+) \sim 11.225$ in all the computations. Since the present model has varying geometrical and velocity scales, then consequently the grid and near-wall refinement will have varying levels of resolution. Hence, to have consistency in modelling approach the scalable wall function displaces the near-wall mesh to a y^+ value of 11.225 which is the transition to the log-law region. This is necessary since epsilon-based models are not ideal for modelling the laminar sub-layer and the scalable approach internally adjusts the mesh to ensure this region is not resolved.

The current simulation was carried out using parametric segregated approach. The biggest benefit to the parametric segregated solver approach is that it uses the optimal iterative solver in each linear sub-step. The segregated solver normally need additional iterations until convergence, however every iteration takes considerably less time than one iteration of the fully coupled approach. This method involves the integration of the governing equations for mass, momentum, energy and turbulence within the computational domain to build algebraic equations for every dependent variable which is unknown. Earlier investigations delineated that RANS based models could accurately predict the heat transfer and fluid flow characteristics in a two-pass channel.

Governing Equations

In this study, air is taken as incompressible with constant physical properties. Present study uses Reynolds averaged Navier-stokes (RANS) equations and energy equations which can be written in the general form as

Continuity Equation:

$$\rho \nabla \cdot (u) = 0 \tag{1}$$

Momentum equation:

$$\rho (u \cdot \nabla) u = \nabla \cdot \left[-pI + (\mu + \mu_T) \nabla u + (\nabla u)^T - \frac{2}{3} \rho kI + F \right] \tag{2}$$

where,

$$\mu_t = \rho C_\mu \frac{k^2}{\varepsilon}$$

Energy equation:

$$\rho C_p u \cdot \nabla T = -\nabla \cdot (k \nabla T) + Q \tag{3}$$

Also, k-ε model adds two additional transport equations and two dependent variables: the turbulent kinetic energy (k), and the dissipation rate of turbulence energy (ε),

Turbulent kinetic energy equation (k):

$$\rho (u \cdot \nabla) k = \nabla \cdot \left[\left(\mu + \frac{\mu_T}{\sigma_k} \right) \nabla k \right] + p_k - \rho \varepsilon \tag{4}$$

Dissipation equation (ε):

$$\rho (u \cdot \nabla) \varepsilon = \nabla \cdot \left[\left(\mu + \frac{\mu_T}{\sigma_\varepsilon} \right) \nabla \varepsilon \right] + C_{e1} \frac{\varepsilon}{k} p_k - C_{e2} \rho \frac{\varepsilon^2}{k} \tag{5}$$

where,

$$p_k = \mu_T \left[\nabla u : (\nabla u + \nabla u^T) \right] + \frac{2}{3} \rho k \nabla \cdot u$$

$$C_\mu = 0.09 \quad \sigma_k = 1 \quad \sigma_\varepsilon = 1.3 \quad C_{e1} = 1.44 \quad C_{e2} = 1.92$$

Boundary Conditions

The incompressible dry air at ambient conditions is selected as working fluid with constant properties. The fluid flow is steady, three-dimensional, and turbulent. Inlet temperature is considered to be uniform at 300K. Inlet fluid velocity was determined by the Reynolds number. Turbulence intensity (5%) and turbulence length scale (7% of channel hydraulic diameter) were selected for the computation. The boundary condition at inlet was set as velocity inlet and boundary condition (outflow) was imposed at the outlet. A constant temperature boundary condition was used for the ribbed bottom surface with other surfaces being adiabatic and no-slip.

Grid Independence Study

By definition, a grid independent solution means, to make the mesh fine in each spatial dimension and run the simulation again. If the solution for the original and the refined mesh are identical, or nearly so, the solution can be assumed to be grid independent. Grid independence study was carried out with smooth two-pass channel with grid consisting of 200000, 250000 and 330000 elements. The values of averaged normalized Nusselt number found by utilizing above grid sizes are compared in Figure 4. The difference in values of averaged normalized Nusselt number using 330000 and 200000 mesh elements is 6.3%. Thus, to maintain balance amid computational time economy and efficiency, a grid size consisting of 250000 elements was chosen for the present analysis. Few areas are finely meshed for better analysis of the results. These are areas of heated bottom ribbed wall.

Data Reduction

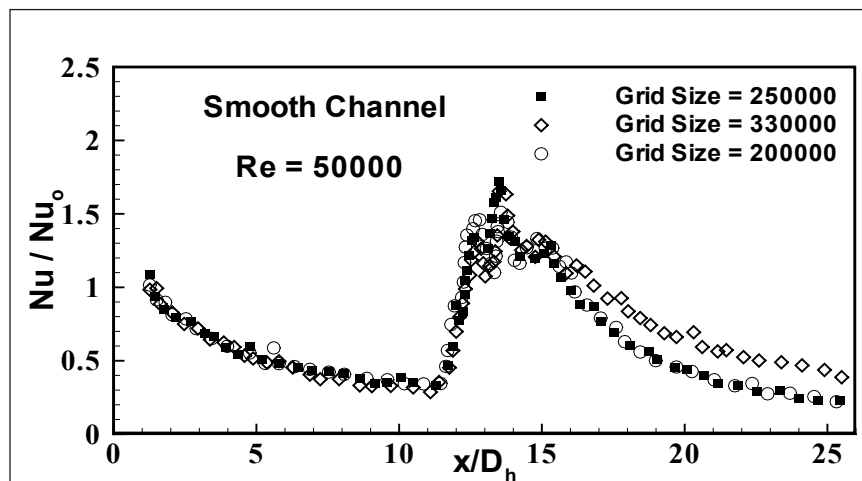


Figure 4. Centerline variation of normalized Nusselt number along Stream-wise direction for three grid sizes

The equation used for determination of heat transfer coefficient over the ribbed surface is as follows:

$$\frac{q''}{(T_w - T_f)} \quad (6)$$

where, q'' stands for heat flux from the heated surface to the surrounding bulk fluid. Velocity of fluid and variations in turbulence are very small and even disappear near the wall. Heat conduction by molecules transports thermal energy in the viscous sub-layer region, which makes the temperature to vary linearly with the distance from the wall (Han and Goldstein., 2008). Hence, the heat flux can be calculated by:

$$q'' = k \frac{\partial T}{\partial n} \quad (7)$$

where, n stands for normal to the surface. Hence, heat transfer coefficient can be calculated from wall temperature, bulk temperature of fluid and heat flux. The local mean bulk fluid temperature is a weighted arithmetic average temperature of fluid and is determined at each stream-wise location using energy balance.

$$Nu = \frac{hD_H}{k} \quad (8)$$

The Nusselt number is normalized by the Dittus- Boelter equation for fully developed turbulent flow in smooth channel.

$$Nu_o = 0.023(\text{Re})^{0.8} \text{Pr}^{0.4} \quad (9)$$

Properties of air were calculated at the mean fluid temperature. Friction factor (f) was determined by equation below:

$$f = \frac{\Delta P D_h}{2 l u_{in}^2 \rho_a} \quad (10)$$

Friction factor is normalized by using Blasius equation given below

$$f_o = 0.316/(\text{Re})^{0.25} \quad (11)$$

Performance Index

The performance evaluation of heat transfer enhancement is carried out in order to determine whether it is beneficial to use augmented surface instead of unaugmented case. In present study augmentation cases involve use of surface mounted ribs in the form of solid ribs, and ribs with square and round perforations at different angles. The relation for performance evaluation given by Gee and Webb (1980) is widely employed for comparison of heat transfer performance of a ribbed duct with smooth duct. This thermal performance index is used under constant pumping power criteria. Higher the value of this parameter, higher is the enhancement in heat transfer at small pressure drop. The thermal performance index (η) is expressed as.

$$Nu = \frac{hD_H}{k} \quad (12)$$

Since, a number of fundamental studies has been conducted with various rib geometries, however, the trend of using square ribs is still used for most of the practical applications, hence can be used for the performance evaluation of the new rib geometries. Some factors, i.e., Nu_{ef} , f_r and η_{ef} are defined below to relate the performance indexes of the perforated ribs with the square rib:

$$Nu_{ef} = \left((Nu_{perforated} - Nu_{solid}) / Nu_{solid} \right) \times 100 \quad (13)$$

$$f_r = \left((f_{solid} - f_{perforated}) / f_{solid} \right) \times 100 \quad (14)$$

$$\eta_{ef} = \left((\eta_{perforated} - \eta_{solid}) / \eta_{solid} \right) \times 100 \quad (15)$$

RESULTS

Following section shows the computational results of heat transfer and fluid flow analysis in a stationary two pass channel with blockages (Cases 1-5) at specified Reynolds number range. Detailed normalized Nusselt number and temperature contours are represented for (Cases 1-5) at the range of Reynolds number studied. All the cases are compared for their heat transfer characteristics on the basis of their enhancement of averaged Nusselt number Nu/Nu_0 . Characteristics of fluid flow in the duct are explained for understanding the mechanism of heat transfer enhancement by the perforated ribs. At last, comparison is also made with square ribs in terms of Nusselt number enhancement, friction factor and thermal hydraulic performance.

Validation of Model

Before carrying out the simulation for a two-pass channel with ribs, few validation runs have been conducted for smooth channel. Figure 5 depicts the comparison of results for distribution of normalized Nusselt number obtained from present simulation with that of Ekkad et al. (1997), Erille et al. (2015) and Jang et al. (2001). Figure 5 shows the close agreement of the present computational results with that of the experimental results of Erille et al., (2015). However at the beginning of the second pass and hereafter lesser value of heat transfer is found. This variation may be because of the different thickness of divider wall and geometry of the bend section than that of Ekkad et al. (1997), Erille et al. (2015) and Jang et al. (2001). These variations bring about a large variation in the flow conditions which directly affects the heat transfer characteristics. The trend of results from the above computation shows close conformity to the previous experimental and computational results. Therefore computation was carried out with the selected turbulence model.

Overall Heat Transfer and Pressure Drop

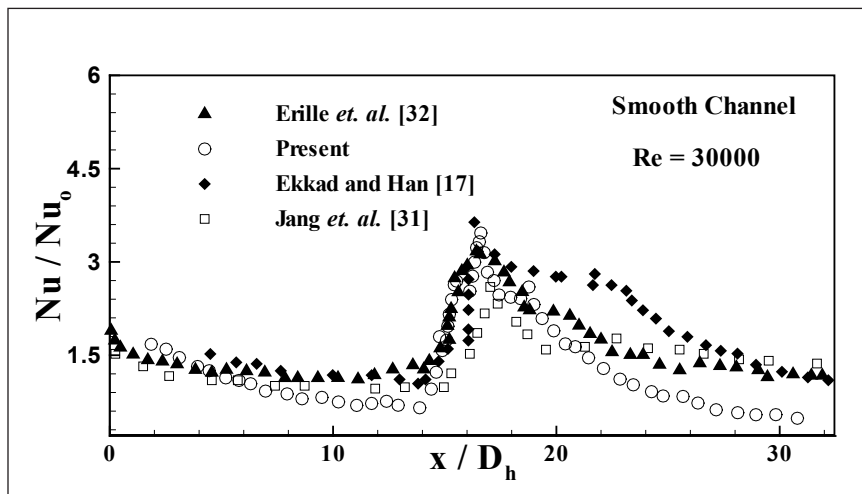


Figure 5. Comparison of normalized Nusselt number with numerical and experimental results

The heat transfer coefficient distribution for perforated rib (Cases 1-5) at Reynolds number range (10000- 50000) and at fixed p/e ratio of 8 have been studied. The detailed analysis of the results reveals that the inter-rib heat transfer distribution is strongly dependent on type of perforation and Reynolds number. To study the fluid flow and heat transfer characteristics of rib roughened channel, it is necessary to understand the secondary flows induced by different perforated rib cases. The fluid flow behavior and turbulence kinetic energy are the major factors that affect the local heat transfer coefficient (Rau et al., 1998). Figure 6 shows the streamline pattern with surface temperature distribution between 3rd and 4th rib of two-pass channel, each perforated case produces a different streamline mapping which

reflects the turbulence features associated with perforated ribs. Typical mapping of the temperature behind solid and perforated rib turbulator is depicted in Figure 7 for Reynolds number equal to 20000. In comparison to solid ribs a significant reduction in temperature at hot spots can be found in case of perforated ribs. Typical temperature contours for (Cases 1-5) is shown in Figure 8.

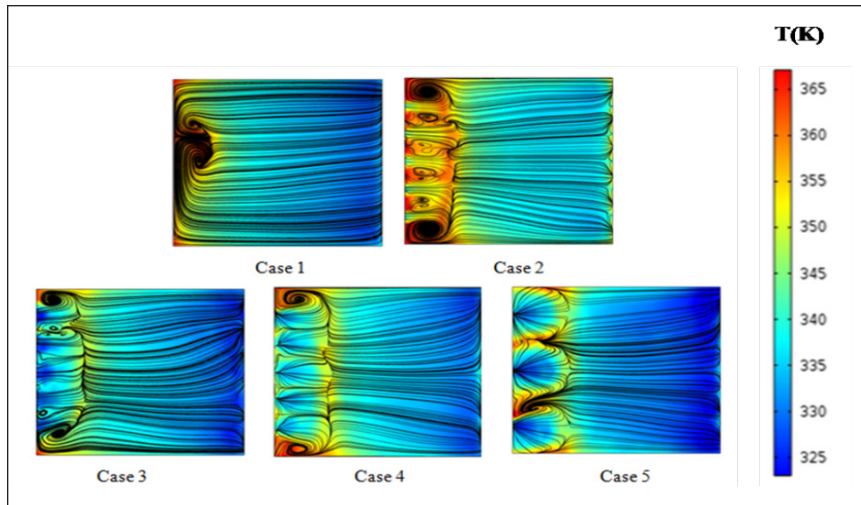


Figure 6. Streamlines with surface temperature distribution for perforated ribs

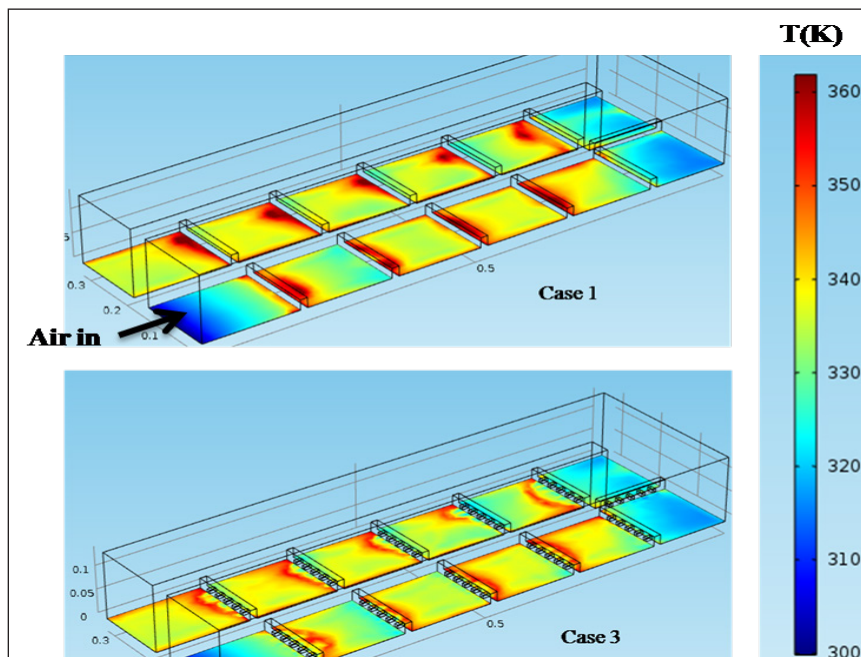


Figure 7. Temperature contours for conventional solid and perforated ribs.

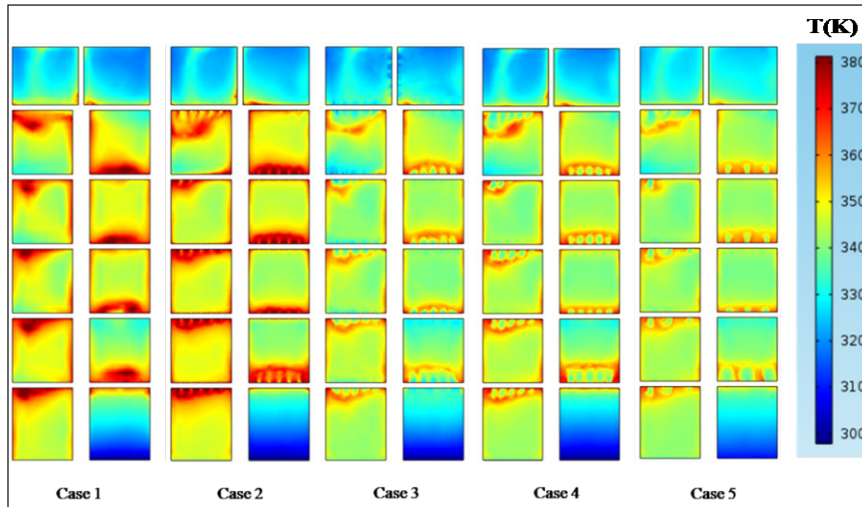


Figure 8. Temperature contour of solid and perforated ribs

Figure 9 provides the mappings of Nu/Nu_0 for (Cases 1-5) for the lowest Reynolds number. The contour plots clearly show the distinct distribution of Nu/Nu_0 corresponding to different perforation cases at same Reynolds number and p/e ratio. Present study displays the effect of perforations towards obviating local hot spot regions, which typically exists just behind the square rib. For most of the Reynolds number perforated ribs provide higher value of normalized Nusselt number than square rib. The modification in heat transfer enhancement can be observed in all the perforated rib cases. This variation in heat transfer enhancement can be possibly because of air flowing through the perforation, causing a modification in secondary flow which breaks the vortices between the ribs. Case 2 ribs gives rise to the formation of a multi wall-jet system, the strength of which decreases quickly so that no more effect is appreciated at a downstream distance. From this location no significant variation of Nusselt number is found indicating that the flow has retrieved its two-dimensional character. However by increasing the perforation angle to 30° fresh air reaches the base of heated plate with more intensity leading to enhancement in heat transfer considerably. Case 3 and Case 5 each have different cooling results. Case 3 ribs show highest heat transfer enhancement, as fluid jets are comparatively very near to the side walls, followed by the Case 5 and Case 4. This becomes clearer when looking at Figure 10 which depicts the heat transfer distribution for (Cases 1- 5).

Figure 11 shows the span-wise averaged normalised Nusselt number ratio at different Reynolds number. The area averaged Nusselt numbers are determined by averaging the local Nusselt numbers over the heated surface on the bottom wall of the channel. Case 2 shows lowest value of Nusselt number augmentation, because the strength of multi wall-jet system formed by the hole at no inclination, decreases quickly so that no more effect is appreciated

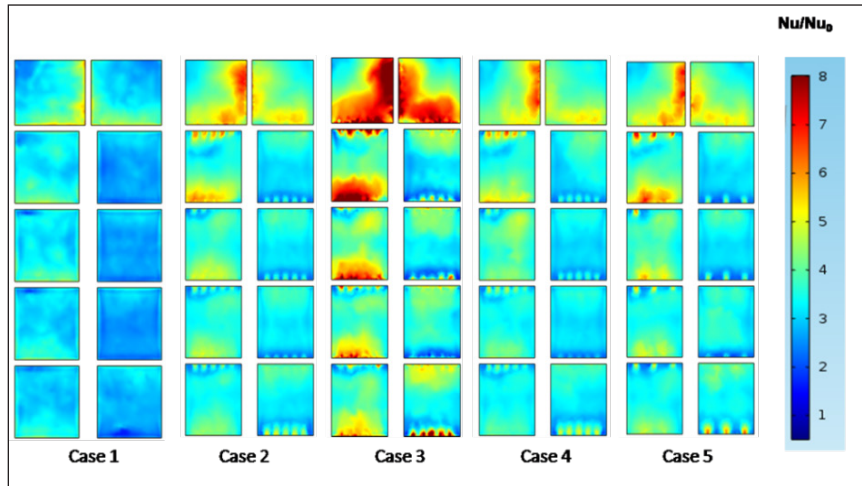


Figure 9. The normalised Nusselt number contours of solid and perforated ribs

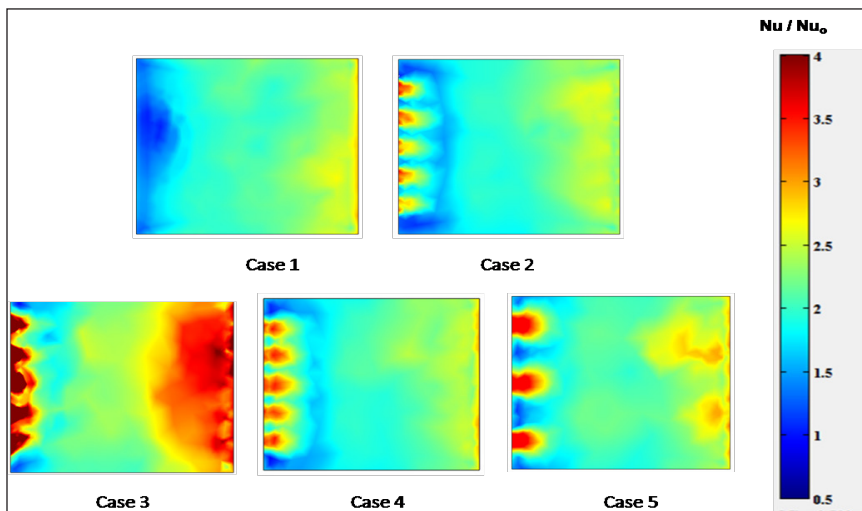


Figure 10. Normalised Nusselt number distribution between third and fourth rib behind perforated ribs

at a downstream distance. The fact that more inclination brings more enhancements is discussed in Figure 11. As depicted in the figure the performance of perforations increases from 0° to 30° and tilted perforations further enhance the normalized Nusselt number, the possible reason could be due to the pointing of jets from both sides of the ribs to the bottom heated wall of the channel. Further analysis of Figure 11 depicts that Nu/Nu_0 is a powerful function of Reynolds number. It decreases with the increase in Re from the maximum at 10000 to the lowest at 50000, which is a well-known behaviour of ribbed ducts (Ekkad et al., 1997; Erelli et al., 2015).

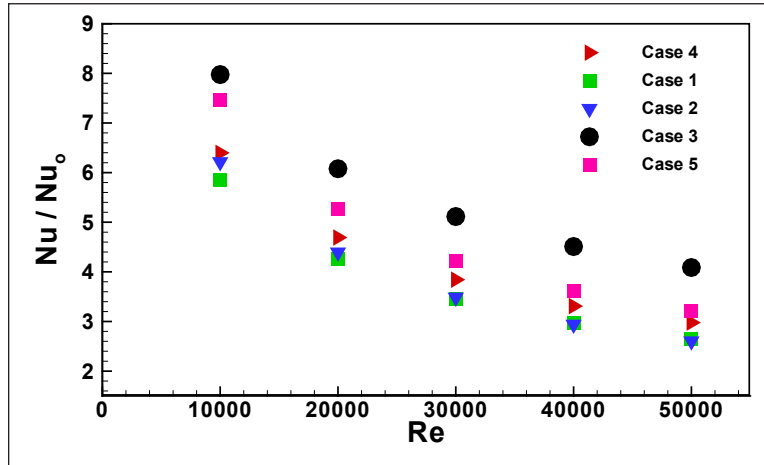


Figure 11. Normalised Nusselt Number Nu/Nu_0 at various Re

The ribs installed in two-pass channel acts as an obstruction to the flow and lead to separation of flow, recirculation and reattachment, therefore leading to the higher pressure loss, and hence higher friction factor for ribbed duct compared to smooth channel at same Reynolds number. The perforated ribs shows higher pressure drop as compared to square ribs except for Case 2 at the present Reynolds number range Figure 12 shows the computational results for f/f_0 as a function of different perforated ribs for different Reynolds numbers at p/e of 8. Friction factor results evidently signify that the installation of ribs lead to pressure drop increment up to 0.89–6.3 % higher than that of the solid ribs under similar flow conditions. Clearly, friction factor is the performance parameter related to pressure penalty. The friction factor ratio increases slightly with the increase in Reynolds number. Inclined holes shows highest friction factors than the ribs with other perforations.

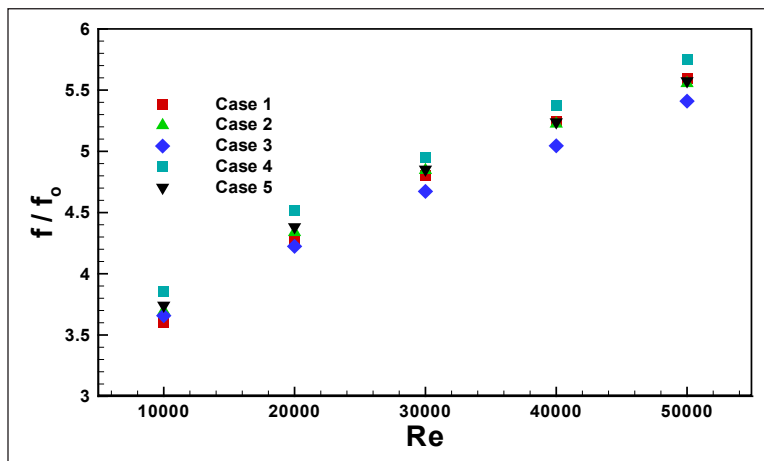


Figure 12. Normalised friction factor f/f_0 at various Re

Figure 13 presents the thermal performance factor for (Cases 1-5) calculated using Eq. (12). It is clear from the figure, that thermal performance factor decreased as the Reynolds number increased. Among the tested perforated blockages, Case 3 showed the highest thermal performance factor. Case 1 and Case 2 shows almost equivalent thermal hydraulic performance. Other cases show performance greater than that of the conventional square rib. The difference in thermal hydraulic performance is more prominent at lowest Reynolds number.

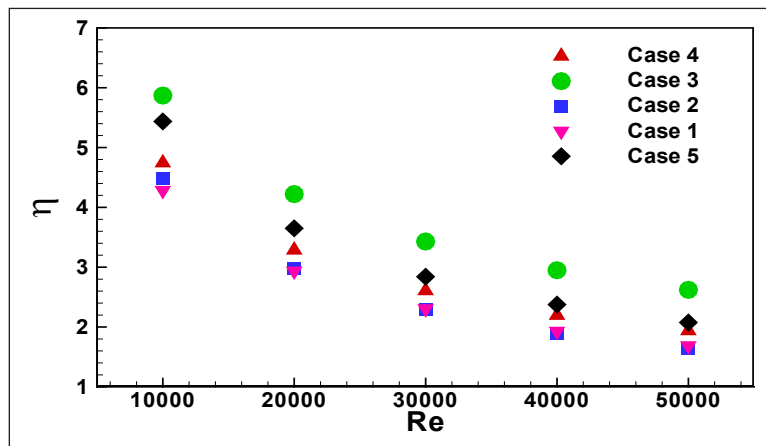


Figure 13. Thermal-hydraulic performances at various Reynolds number

Table 2 shows the comparison of Nu_{ef} , f_r and η_{ef} for different Reynolds number at fixed p/e of 8. For most of the Reynolds number, perforated ribs show better values Nu_{ef} , f_r and η_{ef} than square ribs. On the contrary, at almost all values of Reynolds number except for Case 3, square ribs perform better than perforated ribs from relative friction factor point of view. Also, Case 3 shows highest value of most of the Nu_{ef} , f_r and η_{ef} for all Reynolds number considered, except the performance in terms of friction factor at lowest Reynolds number is found to be less than the square rib.

Table 2
Comparison of relative performance indexes against square rib at different Re for different perforated cases

P/e	Cases	Re				
		10000	20000	30000	40000	50000
8	Case 2	Nu _{EF}	Nu _{EF}	Nu _{EF}	Nu _{EF}	Nu _{EF}
		f _R	f _R	f _R	f _R	f _R
		η _{EF}	η _{EF}	η _{EF}	η _{EF}	η _{EF}
	Case 3	20.07	19.91	21.2	22.80	23.54
		2.30	1.52	0.89	-0.36	-0.69
		0.31	4.07	5.86	3.03	0.99
	Case 4	28.3	38.30	46.7	53.40	57.05
		1.35	-0.93	-2.40	-3.50	-3.09
		20.92	52.77	53.05	49.52	55.10
	Case 5	-5.80	-3.28	-0.94	0.73	1.40
		6.30	5.40	2.90	2.10	2.40
		5.33	14.55	27.51	29.93	32.39
	Case 6	2.94	6.72	10.23	12.60	14.40
		0.40	0.40	1.02	-0.12	-0.38
		3.88	21.34	32.50	33.68	34.99

CONCLUSION

Numerical simulations for steady-state heat transfer and pressure drop measurements behind two dimensional perforated ribs in a two-pass channel were performed. Average Nusselt number and overall friction factor results were obtained for Cases 1 to 5 at different Reynolds numbers. The area of perforations was kept same. The mapping of the heat transfer coefficient provides a useful visualization support to interpret the complexity of the resulting flow. The results are summarized below for the conditions and geometries under which the simulations were conducted:

1. The study compared the average heat transfer coefficients obtained with five perforation designs in rib turbulators. Fraction of the air swept through the perforated rib and interacted with the recirculation bubble generated behind the rib by the impingement of the upper free stream on the wall. As a consequence, the hot spot area occurring in the region just behind a solid-type rib did not exist anymore in the corresponding region of the perforated turbulator.
2. Perforations in the blocks enhanced the heat transfer coefficient on the wall segments between the ribs by 1.4-57 % than that of the flow through the channel with conventional solid ribs at the same flow rate.
3. Inclined perforations in ribs performed better in terms of heat transfer coefficients. Depending upon the inclination angle, inclination may lead to 18.3 to 25.4% increase in heat transfer performance than the conventional solid ribs.

4. Perforated blocks led to larger pressure drop as compared to conventional square blocks.
5. For a given pumping power, Case 3 generated highest enhancement of heat transfer than that of the square ribs.

REFERENCES

- Acharya, S., Dutta, S., Myrum, T. A., & Baker, R. S. (1993). Periodically Developed Flow and Heat Transfer in a Ribbed Duct. *International Journal of Heat and Mass Transfer*, 36(8), 2069–2082.
- Ahn, H. S., Lee, S. W., Lau, S. C., & Banerjee, D. (2007). Mass (heat) transfer downstream of blockages with round and elongated holes in a rectangular channel. *Journal of Heat Transfer*, 129(12), 1676–1685.
- Ali, M. S., Tariq, A., & Gandhi, B. K. (2016). Role of chamfering angles and flow through slit on heat transfer augmentation behind a surface-mounted rib. *J. Heat Transfer* 138(11), 1-16.
- Armellini, A., Coletti, F., Arts, T., & Scholtes, C. (2008). Aero-thermal investigation of a rib roughened trailing edge channel with crossing-jets. Part I: flow field analysis. In *Proceedings of ASME Turbo Expo* (pp. 615-661). Berlin, Germany.
- Buchlin, J. M. (1993). Heat transfer behind a rectangular cylinder in a boundary layer. *Journal of Applied Fluid Mechanics*, 4(1), 137-149.
- Chamoli, S., & Thakur, N. S. (2015). Thermal Behaviour in Rectangular Channel Duct Fitted with V- Shaped Perforated Baffles. *Heat Transfer Engineering*, 36(5), 471- 479.
- Chung, H., Park, J. S., Sohn, H. S., Rhee, D. H., & Cho, H. H. (2013). Trailing edge cooling of a gas turbine blade with perforated blockages with inclined holes. In *Proceedings of ASME Turbo Expo 2013: Turbine Technical Conference and Exposition* (pp. V03AT12A043-V03AT12A043). San Antonio, Texas, USA.
- Coletti, F., Armellini, A., Arts, T., & Scholtes, C. (2008). Aero-thermal investigation of a rib roughened trailing edge channel with crossing-jets, Part II: heat transfer analysis. In *Proceedings of ASME Turbo Expo* (pp. 663-673). Berlin, Germany.
- Ekkad, S. V., & Han, J. C. (1997). Detailed heat and mass transfer distribution in a two-pass Square channel with rib turbulators. *International Journal of Heat and Mass Transfer*, 40(11), 185-193.
- Erelli, R., Saha, K., & Panigrahi, P. K. (2015). Influence of turn geometry on turbulent fluid flow and heat transfer in a stationary two-pass square duct. *International Journal of Heat and Mass Transfer*, 89, 667-684.
- Gao, B., Bi, Q., & Gui, M. (2016). Experimental Performance Comparison of Shell Side Heat Transfer for Shell-and-tube Heat Exchangers with Different Helical Baffles. *Heat Transfer Engineering*, 37(18), 1566-1578.
- Gee, D. L., & Webb, R. L., (1980). Forced convection heat transfer in helically rib roughened tubes. *International Journal of Heat and Mass Transfer*, 23(8), 1127–1135.
- Han, J. C., Dutta, S., & Ekkad, S. (2012). *Gas turbine heat transfer and cooling technology*. New York, USA: Taylor and Francis Group, CRC Press.
- Han, J. C., Park, J. S., & Lei, C. K. (1985). Heat Transfer Enhancement in Channels with Turbulence Promoters. *Journal of Engineering for Gas Turbines and Power*, 107(3), 628-635.

- Han, S., & Goldstein, R. J. (2008). The heat/mass transfer analogy for a simulated turbine blade. *International Journal of Heat and Mass Transfer*, 51(21-22), 5209-5225.
- Jang, Y. J., Chen, H. C., & Han, J. C. (2001). Computation of flow and heat transfer in two pass channels with 60° ribs. *Journal of Heat Transfer*, 123(3), 563–575.
- Jeng, T. M., Tzeng, S. C., & Xu, R., (2013). Fluid visualization and heat transfer tests in an 180° round turned channel with a perforated divider. *International Communications in Heat and Mass Transfer*, 44, 45-51.
- Liou, T. M., & Chen, S. H. (1998). Turbulent Heat and Fluid Flow in a Passage Disturbed by Detached Perforated Ribs of different heights. *Journal of Heat Mass Transfer*, 41(12), 1795-1806.
- Liou, T. M., & Hwang, J. J. (1994). Augmented Heat Transfer in a rectangular channel with permeable ribs mounted on one wall. *Journal of Heat Transfer*, 116(4), 912-920.
- Liou, T. M., Chen, C. C., & Tsai, T. W. (2000). Heat Transfer and Fluid Flow in a square duct with 12 different shaped vortex generators. *Journal of Heat Transfer*, 122(2), 327-335.
- Multiphysics, C. O. M. S. O. L. (2014). *Heat transfer module user's guide. COMSOL version, 4*. Burlington, MA: COMSOL Inc.
- Qayoum, A., & Panigrahi, P., (2018). Experimental investigation of heat transfer enhancement in a two-pass square duct by permeable ribs. *Heat Transfer Engineering*, 1-2. doi: 10.1080/01457632.2018.1436649
- Rau, G., Cakan, M., & Moeller, D. (1998). The Effect of Periodic Ribs on the Local Aerodynamic and Heat Transfer Performance of a Straight Cooling Channel. *ASME*, 120(2), 368–375.
- Sharma, N., Tariq, A., & Mishra, M., (2017). Detailed Heat Transfer Investigation inside a Rectangular Duct with an Array of Ventilated Rib Turbulators. In A. K. Saha, D. Das, R. Srivastava, P. K. Tanigrahi & K. Muralidhar (Eds.), *Fluid Mechanics and Fluid Power –Contemporary Research* (pp. 775-784). India: Springer.
- Shin, S., & Kwak, J. S. (2008). Effect of hole shape on the heat transfer in a rectangular duct with perforated blockage walls. *Journal of Mechanical Science Technology*, 22(10), 1945– 1951.
- Tariq, A., Panigrahi, P. K., & Muralidhar, K. (2004). Flow and Heat Transfer in the Wake of a Surface Mounted Rib with a Slit. *Experiments in Fluids*, 37(5), 701–719.
- Tariq, A., Singh, K., & Panigrahi, P. K. (2003). Flow and Heat Transfer in Rectangular Duct with Single Rib and Two Ribs Mounted on the Bottom surface. *Journal of Enhanced Heat Transfer*, 10(2), 171-198.
- Thianpong, C., Eiamsa-ard, P., & Eiamsa-ard, S., (2012). Heat transfer and thermal performance characteristics of heat exchanger tube fitted with perforated twisted-tapes. *Heat Mass Transfer*, 48(6), 881-892.
- Webb, R. L., & Eckert, E. R. G. (1972). Application of Rough Surfaces to Heat Exchanger Design. *International Journal of Heat Mass Transfer*, 15(9), 1647– 1658.
- Webb, R. L., (1994). *Principles of enhanced heat transfer*. New York, USA: John Wiley and Sons.
- Yuan, Z. X., Tao, W. Q., & Yan, X. T. (2003). Experimental Study on Heat Transfer in Ducts with Winglet Disturbances. *Heat Transfer Engineering*, 24(2), 76-84.

APPENDIX**Nomenclature**

D_h	Hydraulic diameter	[m]
e	Rib height	[m]
F	Body force vector	[N/m ³]
f	Friction factor	
f_r	Friction factor reduction compared to square rib	
h	Heat transfer coefficient	[W/m ² K]
K	Thermal conductivity	[W/mK]
L	Channel length	[m]
Nu	Nusselt number	
Nu_{ef}	overall Nusselt number enhancement factor compared to square rib	
P	Rib pitch	[m]
p	Pressure	[Pa]
q''	Heat flux	[W/m ²]
Re	Reynolds number	$[\rho u_{in} D_h / \mu]$
u	Fluid velocity	[m/s]

Subscripts

f	Fluid
in	inlet
o	From Dittus-Boelter Coorelation
w	wall

Greek symbols

ρ_a	Density of air [kg/m ³]
η	Thermo-hydraulic performance
η_{ef}	Factor for performance enhancement compared to square rib
μ	Dynamic viscosity [kg/ms]

